Front. Earth Sci. 2013, 7(3): 282–294
DOI 10.1007/s11707-013-0372-0

RESEARCH ARTICLE

Jet-like features of Jiulongjiang River plume discharging into the west Taiwan Strait

Daifeng WANG[1], Quan'an ZHENG[1,2], Jianyu HU (✉)[1]

1 State Key Laboratory of Marine Environmental Science, College of Ocean and Earth Sciences, Xiamen University, Xiamen 361005, China
2 Department of Atmospheric and Oceanic Science, University of Maryland, College Park, MD 20742, USA

Abstract In-situ data from the summer cruise of 2010 in the west Taiwan Strait are used to study the spatial distribution of the Jiulongjiang River plume (JRP). The results show that in the 2 m layer, the JRP debouches into the west Taiwan Strait in the form of jets, with one branch through the Xiamen Bay (Xiamen JRP) and another through the channel between Jinmen and Weitou (JinWei JRP). Driven by the summer southwesterly monsoon, the upwelling-related Dongshan low temperature and high salinity water flows northeastward in the form of a jet as well. To a certain degree, the Dongshan low temperature and high salinity jet restricts the Xiamen JRP from spreading further offshore and drags the JinWei JRP northeastward at the same time. Meanwhile, a terrestrial dissolved organic matter (DOM) distribution model on the basis of molecular collision theory in thermodynamics and statistical physics is applied to analyze the Moderate Resolution Imaging Spectroradiometer (MODIS) turbidity data. The correlation coefficient of the theoretical model to the MODIS turbidity data reaches 0.96 (significant at a 95% level of confidence). The result clarifies the dynamic mechanism for the turbidity distribution characteristics. It is the salinity in macro-scale that plays a decisive role in the turbidity variability in the coastal water. This suggests that the satellite-derived turbidity data can be used as an indicator to show the spreading patterns of the JRP. Based on the turbidity data from 2003 to 2011, we conclude that there are four main spreading patterns of the JRP.

Keywords Jiulongjiang River plume, jet current, terrestrial DOM, MODIS data, Taiwan Strait

1 Introduction

The Jiulongjiang River is the second largest river in Fujian Province in southeastern China, located on the west coast of the Taiwan Strait. It consists of three tributaries: the North Brook, the West Brook, and the South Brook (Fig. 1). The North Brook is the main stream with annual mean runoff reaching 8.9×10^9 m^3, and the West Brook has an annual mean runoff of 3.7×10^9 m^3. The combined peak discharge of the two brooks in the wet season from April to September accounts for 74% of the total annual runoff. The Jiulongjiang River runoff is mainly affected by precipitation, and heavy flooding may be caused by rainstorms and typhoon rainfall (Guo et al., 2011).

The river discharges to coastal waters with a large amount of nutrients, sediments, and contaminants have profound influence on the sensitive coastal marine ecosystems. Hydrodynamically, the fresh river water spreading over the saline seawater forms a body of plumose low salinity water, which is generally called plume. The river plume constitutes an important dynamic component of the coastal circulation. Due to ecological and dynamical importance, it is necessary to have a good understanding of river plumes. However, to a great extent, interest in river plumes has only focused on large rivers, such as the Yangtze River (Mao et al., 1963; Lie et al., 2003; Kim et al., 2009; Wu et al., 2011; Rong and Li, 2012), the Mississippi River (Ortner et al., 1995; Schiller et al., 2011), and the Columbia River plume (Hickey et al., 2005; Liu et al., 2009a, 2009b; MacCready et al., 2009). For the small rivers such as the Jiulongjiang River, the previous investigators mainly paid attention to the area from the river mouth to the Xiamen Bay, focusing on the distribution characteristics of the salinity, the salinity front, the changes in nutrients and the impact of tides to the characteristics (Zhang et al., 1999; Chen et al., 2002; Luo et al., 2011, 2012). The sediment transport, chlorophyll *a* and primary productivity, and current fields were also

Received January 18, 2013; accepted March 6, 2013

E-mail: hujy@xmu.edu.cn

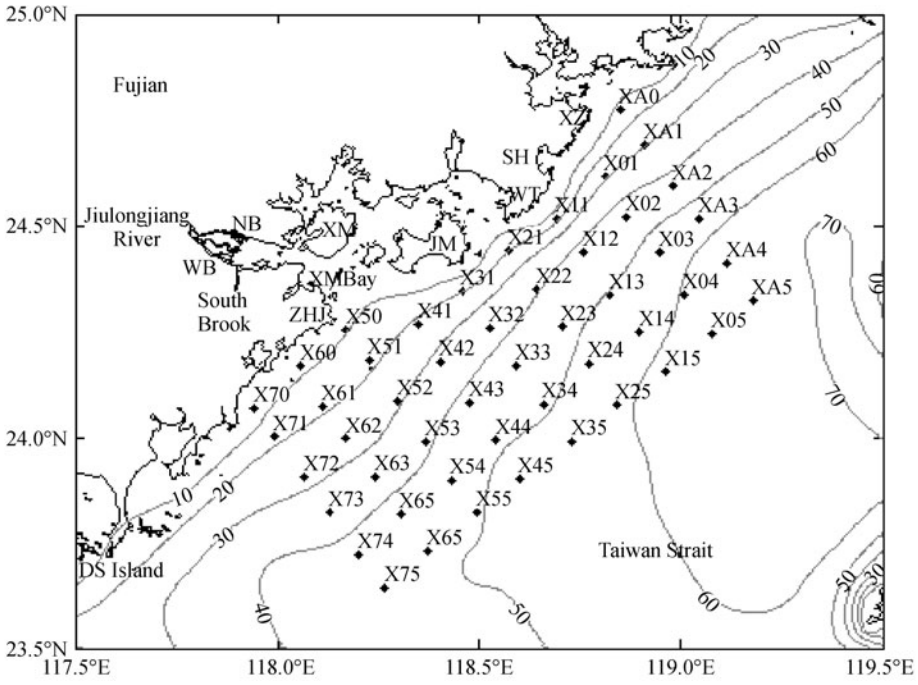

Fig. 1 Study area. Dots with codes represent CTD stations. Bathymetry units are in meter. XZ, SH, WT, JM, XM, NB, WB, ZHJ and DS represent Xiangzhi, Shenhu, Weitou, Jinmen, Xiamen, North Brook, West Brook, Zhenghaijiao, and Dongshan, respectively.

considered. In addition, the previous works on analyzing the data of temperature and salinity in the Taiwan Strait (Chen et al., 2002; Chen et al., 2009) involved the hydrological characteristics of the Jiulongjiang River plume (JRP). However, the dynamical characteristics of the JRP remain unclear. This study aims to clarify the dynamical characteristics of the JRP using the cruise data observed with a conductivity-temperature-depth (CTD) profiler, the reanalyzed satellite turbidity data, and the theory of fluid mechanics, and that of molecular collision in thermodynamics and statistical physics.

We introduce the data used in this paper in Section 2, including the cruise data in summer 2010 and the Moderate Resolution Imaging Spectroradiometer (MODIS) reanalyzed turbidity data. The analysis and interpretation of the in-situ salinity distribution are given in Section 3. Next, we investigate the distribution of terrestrial dissolved organic matter (DOM) of the JRP using the MODIS reanalyzed turbidity data in Section 4. We do a statistical analysis of the turbidity data by using turbidity as an indicator of plume in Section 5. Section 6 presents a summary.

2 Data

The in-situ data used in this study are from the cruise observations carried out from June 28 to 30 in 2010 in the west Taiwan Strait, including the temperature, salinity, and density anomaly originally measured with a CTD profiler. As shown in Fig. 1, the survey area is mapped by the CTD profiler casts at 49 sampling stations along 9 cross-shelf transects. The distance between two neighboring transects is about 18 km, and that between two adjacent stations varies from 8 to 15 km. At each station, the CTD data were measured continuously from the sea surface to the depth close to the bottom with a vertical resolution of 1 m. Because the lengths of transects are different, the sampling time was from 4 to 5 h per transect, and the entire sampling was accomplished in three days. The water depth in the survey area changes from 10 to 60 m (Fig. 1).

In the meantime, based on the MODIS level 2 LAC (Large Area Collectors) data downloaded from the data dissemination center of US NASA (National Aeronautics and Space Administration) Goddard Space Flight Center (GSFC)[1)] and the algorithms used by Huang et al. (2008), the turbidity data is calculated from 2003 to 2011 with a spatial resolution of 1 km.

3 Cruise data analysis and interpretation

3.1 Spatial distribution of the JRP

We use the cruise data to map the distributions of the salinity and the temperature in 2 m layer and the salinity at depths of 7 and 10 m. The results are shown in Figs. 2 and

1) http://oceancolor.gsfc.nasa.gov/

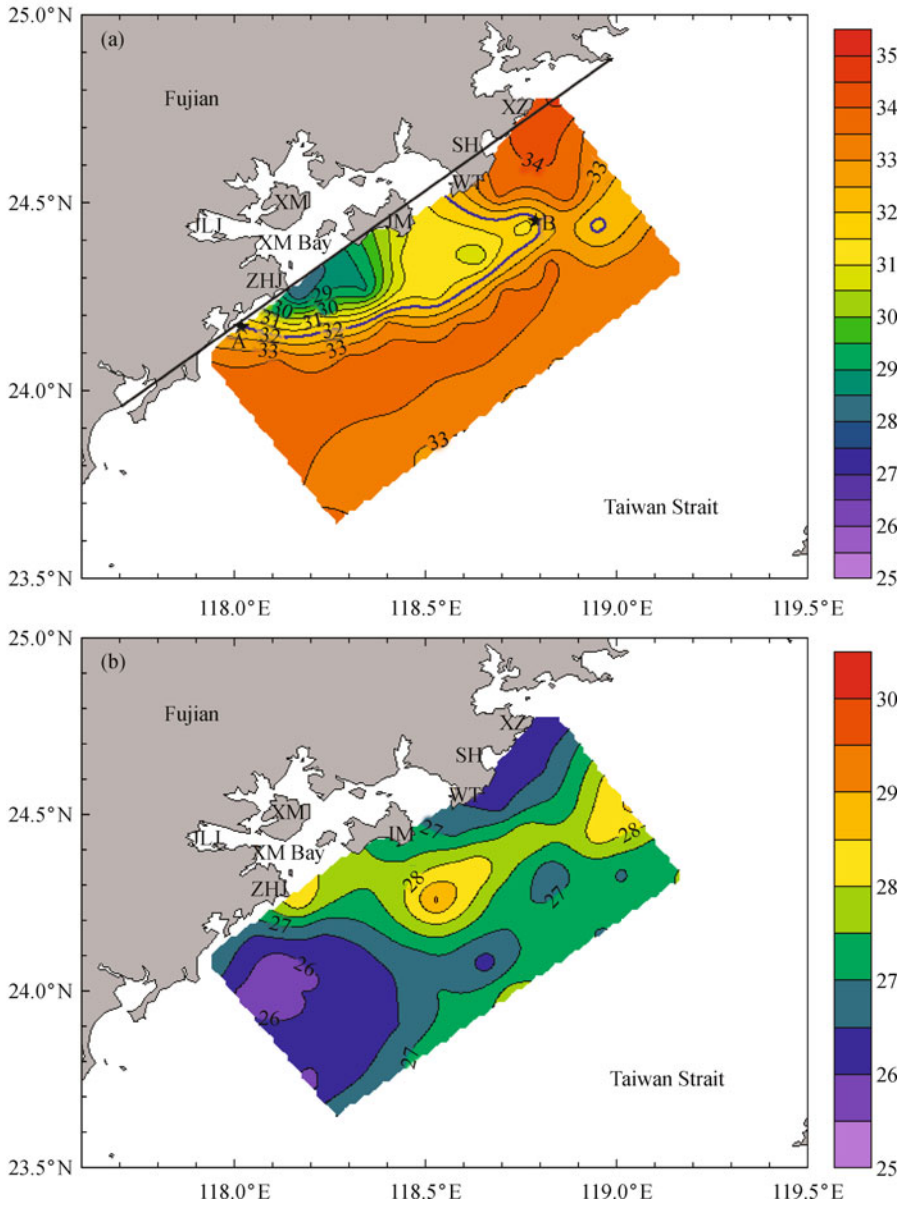

Fig. 2 Distributions of the salinity (a) and the temperature (b) at the depth of 2 m. Blue curve represents the 32 isohaline. Pentagrams represent the locations of points A (24.16°N, 118.00°E) and B (24.45°N, 118.79°E). Black bold line represents the general direction of coastline. In this figure, XZ, SH, WT, JM, XM, JLJ, and ZHJ represent Xiangzhi, Shenhu, Weitou, Jinmen, Xiamen, the Jiulongjiang River, and Zhenghaijiao, respectively.

3, respectively. Following the definition of the Yangtze River plume (Mao et al., 1963), we define the 32 isohaline contour as the boundary of the JRP.

From Fig. 2, one can see that under the influence of topography, the JRP debouches into the west Taiwan Strait through the Xiamen Bay and the channel between Jinmen and Weitou with high temperature and low salinity, varying from 25.7°C to 29.0°C and from 28.1 to 32.0, respectively. The maximum width between the JRP boundary (32 isohaline) and the coastline is about 31.5 km, with the direction of coastline defined as the black bold line shown in Fig. 2(a). The most southwestern and northeastern edges reach the points of A and B (Fig. 2(a)), respectively, and the two points are approximately 86.3 km apart.

In the survey area, driven by the summer southwesterly monsoon, the sea water in the Dongshan upwelling zone (Chen et al., 1982; Hong et al., 2009a; Zhang et al., 2011) flows northeastward, so that there is a low temperature and high salinity tongue (Dongshan low temperature and high salinity water) running southwest-northeastward as shown in Fig. 2. The tongue axis is generally at an angle of 9° to the direction of coastline. After entering into the sea, the JRP interacts with the tongue, making the isohalines become dense at the interaction zone. The horizontal

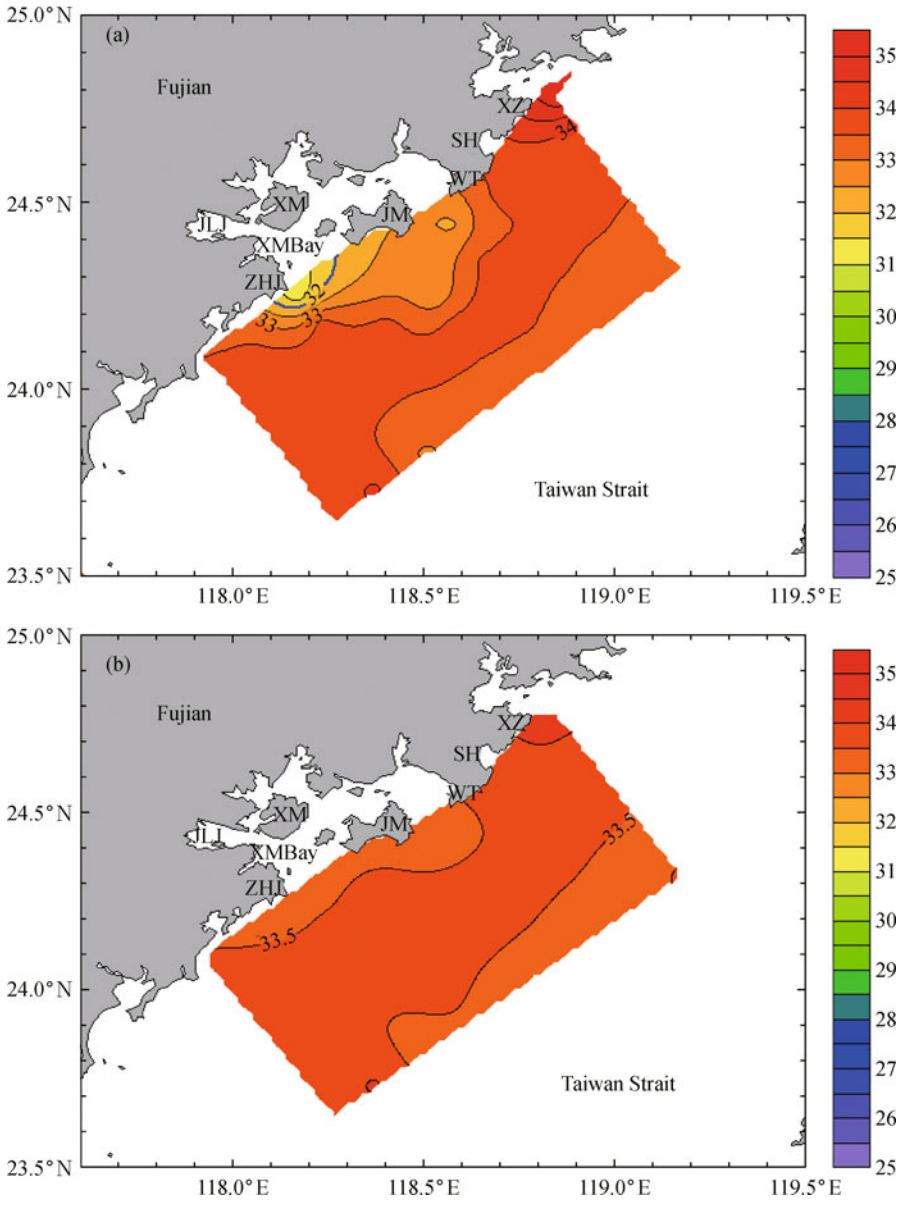

Fig. 3 Distributions of the salinity at 7 m (a) and 10 m (b). Blue bold line represents the 32 isohaline. In this figure, XZ, SH, WT, JM, XM, JLJ, and ZHJ represent Xiangzhi, Shenhu, Weitou, Jinmen, Xiamen, the Jiulongjiang River and Zhenghaijiao, respectively.

salinity gradient reaches 0.250/km, greatly exceeding the criterion of 0.018/km for a salinity front (Hong et al., 2009b).

There is also a low temperature and high salinity tongue near the Xiangzhi-Weitou coastal area which is closely related to the local upwelling. The JRP interacts with the tongue, making the horizontal salinity gradient reach 0.180/km in the upwelling divergence region and forming salinity fronts.

A river plume is usually characterized by a stable stratification with plume-induced fronts surfacing offshore (Chao and Boicourt, 1986). The maximum horizontal salinity gradient of the JRP discharging into the west Taiwan Strait through the Xiamen Bay (Xiamen JRP) reaches 0.365/km. So we can conclude that the plume water with a salinity front is formed near the Xiamen Bay mouth. There are two low salinity tongues in the plume: one is in the southwestward direction with an angle of 151° to the direction of coastline, and the other is perpendicular to the direction of coastline, pointing southeastward.

The low salinity tongue of the JRP entering into the west Taiwan Strait through the channel between Jinmen and Weitou (JinWei JRP) is sandwiched by high salinity waters on both shallow and deep water sides. The high salinity waters originate from the coastal upwelling near the Xiangzhi-Weitou coastal area and the Dongshan low temperature and high salinity water, respectively. Isohalines on both sides of the JRP tongue are dense, with maximum horizontal salinity gradients reaching 0.240/km on the shallow water side and 0.180/km on the deep water

side. This implies that the JinWei JRP forms a plume with a salinity front.

Vertically, at the 7 m layer, the signal of the JRP also exists as shown in Fig. 3(a), but the patterns differ from that at the 2 m layer. The 7 m layer of the JRP spreads near the Xiamen Bay mouth, with the maximum width between its boundary (32 isohaline) and the coastline equaling 7.2 km and the width between the most southwestern and the most northeastern edges approximating 17.5 km. The tongue axis of the JRP in the 7 m layer coincides with that of the JRP running southwestward in the 2 m layer, while the tongue axis becomes a little shorter in the 7 m layer. Thus, it is clear that the coverage of the JRP in this layer becomes narrower. The maximum horizontal salinity gradient of the JRP in the 7 m layer reaches 0.243/km, which indicates that the plume water with a front is formed. Different from that in the 2 m layer, the direction of low salinity tongue in the plume is single in the 7 m layer. At the 10 m layer, the plume signal disappears (Fig. 3(b)), implying that the JRP is mainly concentrated in the upper layers from the sea surface to the depth less than 10 m.

3.2 Interpretation to the JRP distribution

3.2.1 Two-dimensional jet

Formally, a two-dimensional jet is a special flow formed by an efflux of fluid from a long and narrow orifice into the same type of fluid as the jet itself, as illustrated in Fig. 4 (Kundu, 1990). Dynamically, the jet is controlled by two conditions (Kundu, 1990). One is the momentum flux preservation, i.e.,

$$M = \rho \int_{-\infty}^{+\infty} u^2 \mathrm{d}y, \tag{1}$$

where ρ is the density of fluid, u is the x-component of velocity, and the coordinate system is defined as that in Fig. 4. The second condition is a similarity solution of the stream function in the form of

$$\psi = ax^{1/3}\tanh\ \eta, \tag{2}$$

where

$$a = \left(\frac{9A_H M}{2\rho}\right)^{1/3}, \tag{3}$$

in which A_H is the horizontal eddy viscosity, and

$$\eta = \frac{y}{bx^{2/3}}, \tag{4}$$

in which

$$b = \left(\frac{48A_H^2\rho}{M}\right)^{1/3}. \tag{5}$$

From Eq. (2), we derive the velocity components of the jet. The x-component or axial velocity is given by

$$u = u_{\max}\mathrm{sech}^2\eta, \tag{6}$$

where $u_{\max}$ is the maximum axial velocity at the center of the jet given by

$$u_{\max} = \frac{a}{b}x^{-1/3} = \left(\frac{3M^2}{32\rho^2 v}\right)^{1/3} x^{-1/3}, \tag{7}$$

and the y-component or transverse velocity is given by

$$v = v_{\max}(2\eta\mathrm{sech}^2\eta - \tanh\ \eta), \tag{8}$$

where $v_{\max}$ is the maximum transversal velocity given by

$$v_{\max} = \frac{a}{3}x^{-2/3}. \tag{9}$$

From these equations, it follows that the dynamics of an ideal two-dimensional jet are characterized by (i) a jet axis that is kept unchanged, (ii) a jet width that increases as $x^{2/3}$, (iii) an x-component velocity that decreases as $x^{-1/3}$, and (iv) a y-component velocity that decreases as $x^{-2/3}$ (Zheng et al., 2004).

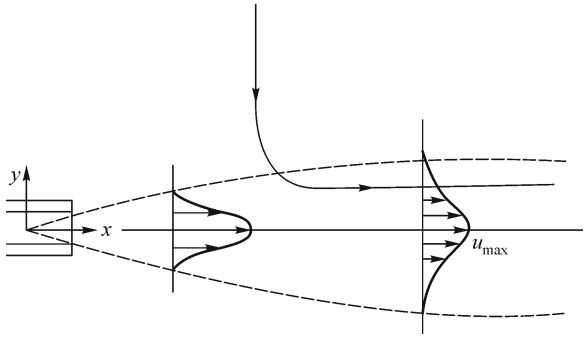

Fig. 4 A scheme of a two-dimensional jet flow (redrawn from Kundu, 1990).

3.2.2 Interpretation to the distribution of JRP

We use density anomaly (ρ_t) data derived from the cruise CTD measurements to calculate the current field structure. If we assume the y-component of velocity is ignored, the following approximate relation stands:

$$\rho_t = -\alpha u(y), \tag{10}$$

where α is a constant to be determined and $u(y)$ represents the x-component of velocity. This means that using density anomaly data we may determine a normalized form of $u(y)$ used for dynamical analysis even though α is unknown (Zheng et al., 2004). In this paper, we choose the JRP tongue axes and the upwelling-related low temperature and

high salinity tongue axis as the *x*-axes, and the lines perpendicular to *x*-axes are *y*-axes.

In order to compare the velocity fields of the JRP with those of the corresponding jet models, we select two transects off Zhenhaijiao-Jinmen and another two transects off Jinmen-Shenhu, defined as T0 (blue line in Fig. 5), T1 (red line in Fig. 5), T2-1 and T2-2 (black lines in Fig. 5), respectively. T0 includes two stations X51 and X60 and one interpolation point (blue dot in Fig. 5) whose density anomaly data is calculated by using linear interpolation based on cruise observations at X50 and X61. T1 includes three stations X31, X41, and X51.Three stations X21, X22, and X23 are on T2-1, while X11, X12, and X13 on T2-2. On the basis of Eq. (10), velocity fields for the above four transects in the 2 m layer are calculated and then normalized by the corresponding maximum axial velocities. Figures 6(a)–6(d) show comparisons of the normalized velocity fields of T0, T1, T2-1, and T2-2 with their corresponding jet model curves. The correlation coefficients are all up to 0.99, at the same time, the normalized velocity fields and corresponding jet theoretical values for each transect have no significant differences with a 95% confidence level based on one-way variance analysis. Thus we conclude that the Xiamen JRP discharges into the west Taiwan Strait in the form of two jets J0 and J1 in the direction of southwestward and southeastward, respectively. The two jet axes are at angles of 151° and 90° to the direction of coastline shown in Fig. 5 as a blue arrow J0 and a red arrow J1, respectively. Meanwhile, the JinWei JRP enters into the west Taiwan Strait also in the form of jet J2 whose axis points northeastward shown as a black arrow J2 in Fig. 5 with an angle of 9° to the direction of coastline.

Similarly, in order to compare the velocity field of the Dongshan low temperature and high salinity water in the 2 m layer with that of the corresponding jet model, we select two transects, T3-1 and T3-2, shown as purple lines in Fig. 5. Stations X60, X61, X62, X63, X64, and X65 comprise T3-1, and T3-2 consists of X12, X13, X14, and X15. The comparisons of the normalized velocity fields of T3-1 and T3-2 to their corresponding jet model curves are shown in Figs. 6(e) and 6(f), respectively. The correlation coefficients are 0.99 (significant at the 95% level of confidence), implying that the Dongshan low temperature and high salinity water enters into the survey area also in the form of jet J3. I.e., J3 is a wind driven coastal upwelling jet and detailed studies of the patterns and dynamics of this kind of jet can be seen in Liu and Weisberg (2007). The axis of J3 points northeastward and is shown as a purple arrow J3 in Fig. 5, with an angle of 9° to the direction of the coastline.

In summary, Fig. 5 shows a sketch of 4 jets (J0–J3) in the 2 m layer. One can see that J3 is wider and longer than other jets, suggesting that the intensity of J3 is the strongest. Second, J2, which is developed by the JinWei JRP, spreads northeastward as it is dragged by J3, without

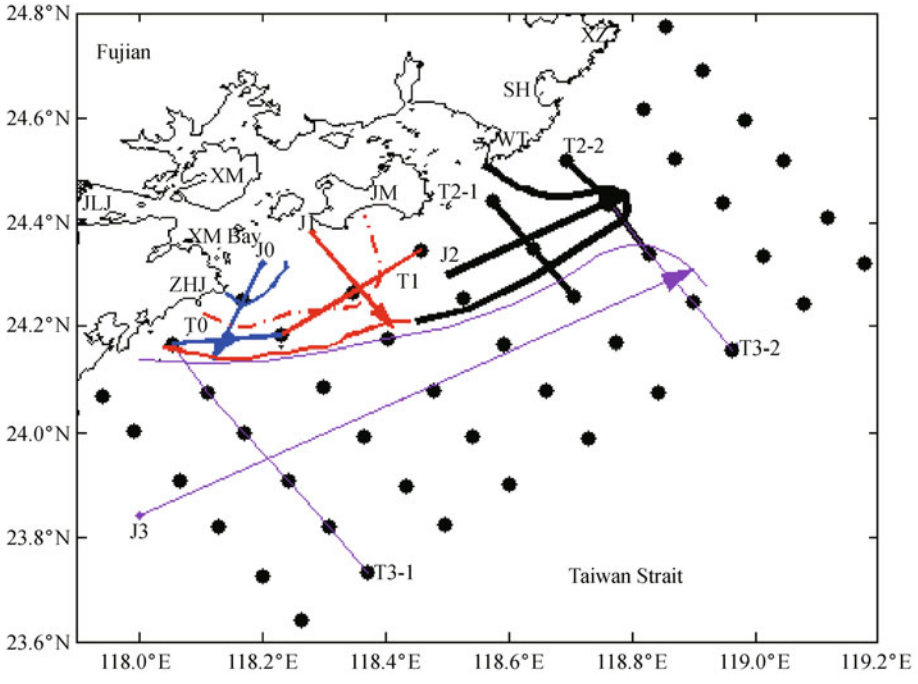

Fig. 5 An interpretation map of Fig. 2. Black solid dots represent stations. The blue solid dot represents an interpolation point. Lines of dots with codes represent transects. Arrows with codes represent axes of jets. The blue curve and red dashed curve represent 28.5 and 30.0 isohalines, respectively. The red solid curve and black curve are the boundary of Xiamen JRP and JinWei JRP, respectively. The purple curve represents the front general location of Dongshan low temperature and high salinity water. In the figure, XZ, SH, WT, JM, XM, JLJ, and ZHJ represent Xiangzhi, Shenhu, Weitou, Jinmen, Xiamen, the Jiulongjiang River, and Zhenhaijiao, respectively.

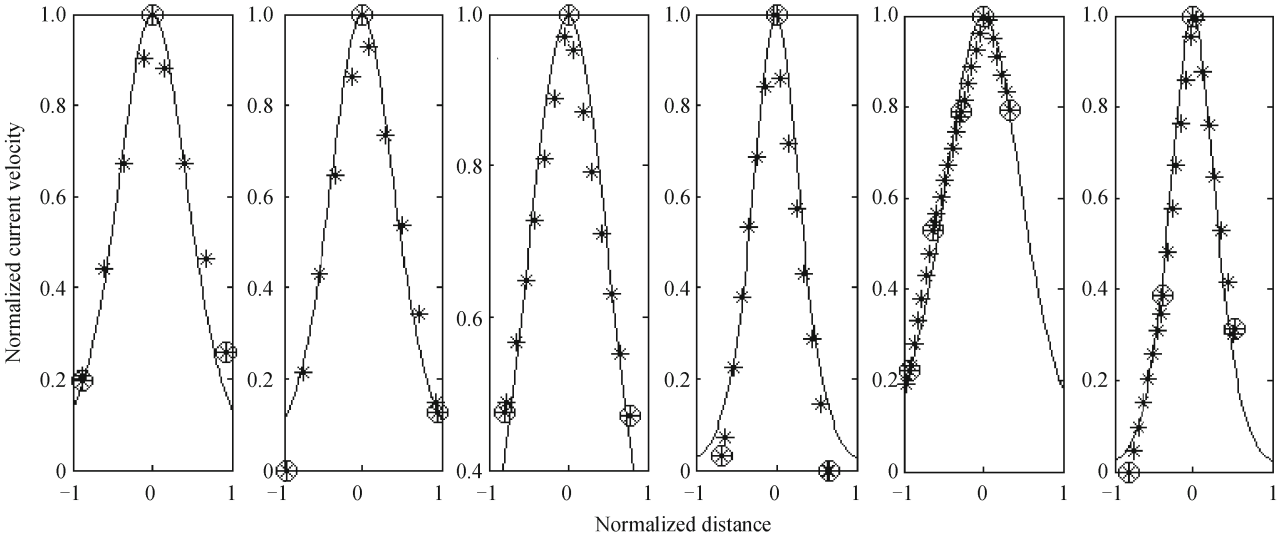

Fig. 6 Jet structures (curves) of velocity fields in the 2 m layer. Circles represent the velocities at the stations. Asterisks represent velocities by interpolation. (a)–(f) are for transects of T0, T1, T2-1, T2-2, T3-1 and T3-2, respectively.

flowing southwestward or southeastward. Third, J3 blocks J0 and J1 for running further offshore.

4 MODIS observations of JRP and the dynamic mechanism

4.1 Spatial distribution of turbidity

High concentrations of particulate matter cause water to appear cloudy due to the absorption and scattering of light. The cloudiness of water is operationally measured as the amount of light transmitted. This quantity is termed turbidity and reported in nephelometric turbidity units (NTU) (Libes, 2009). Suspended particulate matter is mainly from phytoplankton and suspended sediment. The former is the main source for open sea, while the latter for offshore waters (Huang et al., 2008).

Figure 7 shows the spatial distribution of the turbidity reanalyzed from the MODIS data on June 28, 2010 during the period of the summer cruise. In general, the turbidity in the nearshore water is higher than that in the open sea. The turbidity in the open sea is more uniformly distributed, with the turbidity less than 0.5 NTU. Seawater with high turbidity near the Xiamen Bay mouth flows northeastward and southwestward at the same time. Furthermore, there is also a stream of seawater with the high turbidity off Weitou flowing northeastward.

4.2 Statistic-thermodynamical model

Based on the molecular collision theory in thermodynamics and statistical physics, Zheng et al. (2008) developed the terrestrial DOM distribution model. The model, verified by cruise data in the Delaware Bay, indicates that the inelastic collision between the terrestrial DOM molecules and dissolved salt ions in seawater is a decisive dynamic mechanism for the rapid loss of terrestrial DOM. In this paper, we apply the model to our survey area. The terrestrial DOM distribution model is given as follows:

$$n_1(x) = \left[n_1(0) + \frac{\rho\,\overline{\theta}_{12}}{\overline{u}} \int_x^0 n_2(x) \mathrm{e}^{\rho\,\overline{\theta}_{11} x/\,\overline{u}} \mathrm{d}x \right] \mathrm{e}^{-\rho\,\overline{\theta}_{11} x/\,\overline{u}}, \tag{11}$$

where n_1 and n_2 are the numbers of DOM and sodium chloride molecules in a unit volume, respectively, ρ is the probability of inelastic collision between the DOM molecules and the charged salt ions, $\overline{u}$ is a mean flow velocity, x is the distance between the point on the x-axis along the flow direction and the origin one with $x = 0$ km, $\overline{\theta}_{11} = 4\sigma_1^2(\pi kT/m_1)^{1/2}$, $\overline{\theta}_{12} = 2\sigma_{12}^2(2\pi kT/m_1)^{1/2}(1 + m_1/m_2)^{1/2}$, σ_1 is the particle size of DOM molecule, σ_{12} is a sum of the particle size of DOM and the radius of sodium chloride, m_1 and m_2 are their masses, k is the Boltzmann constant, and T is absolute temperature. Here n_1 depends on the turbidity, and n_2 on the salinity, $n_1(0)$ is an initial value of n_1.

In this paper, we choose the axis of high turbidity as the x-axis, which is shown as a black curve with an origin at the black point O in Fig. 7. In order to determine the salinity-related parameter n_2, we use a curve fitting method to establish a function of the salinity versus the distance along x-axis. We choose 11 data points on x-axis for curve fitting, which are stations X50, X41, X31, one point on connecting line of X21 and X22, and other seven points on

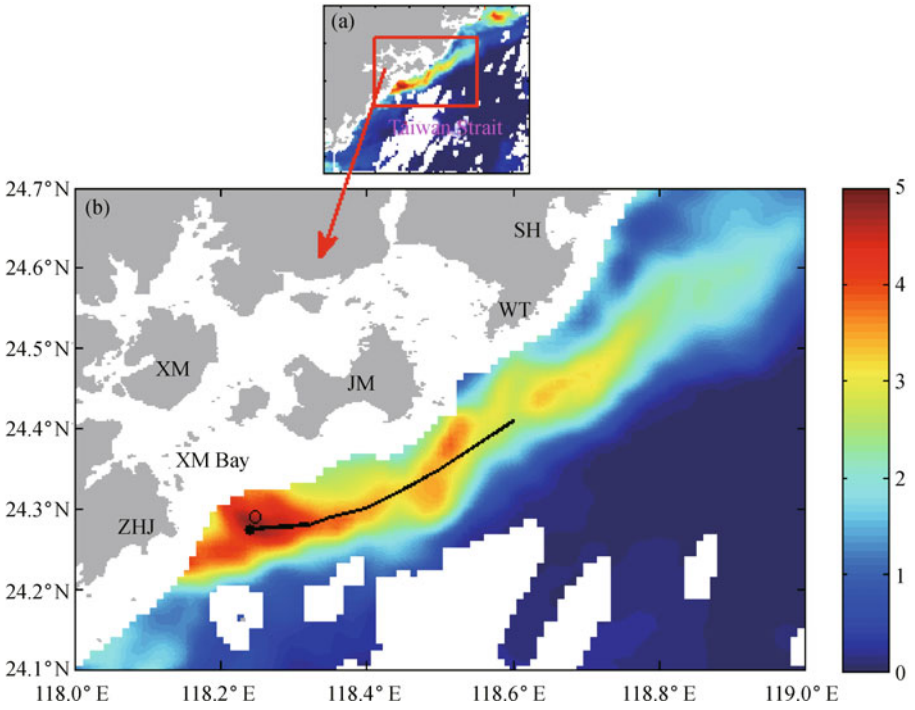

Fig. 7 Turbidity distribution derived from the MODIS observation on June 28, 2010. The black curve represents the axis of high turbidity. Point O is chosen as the origin. SH, WT, JM, XM, and ZHJ represent Shenhu, Weitou, Jinmen, Xiamen, and Zhenhaijiao, respectively.

x-axis. The salinity values of the first three points are taken from cruise observations, and the other points are calculated by Kriging interpolation.

As shown in Fig. 8, we fit salinity distribution with a linear function, $n_2 = b_1 x + b_2$ in which $b_1 = 0.08$ and $b_2 = 28.08$. And the correlation coefficient is 0.91 (significant at the 95% level of confidence).

Substituting the linear function of n_2 into Eq. (11) yields

$$n_1(x) = \left[n_1(0) - \frac{\overline{\theta}_{12}}{\overline{\theta}_{11}}\left(\frac{b_1\,\overline{u}}{\rho\,\overline{\theta}_{11}} - b_2\right)\right] \mathrm{e}^{-\rho\,\overline{\theta}_{11x}/\,\overline{u}}$$

$$-\frac{\overline{\theta}_{12}}{\overline{\theta}_{11}}\left(b_1 x + b_2 - \frac{b_1\,\overline{u}}{\rho\,\overline{\theta}_{11}}\right). \qquad (12)$$

The normalized form of $n_1(x)$, i.e., $n_1(x)/n_1(0)$, is defined as the turbidity index, and then its distribution derived from Eq. (12) along x-axis is given as curves shown in Fig. 9. The parameters are reasonably taken as follows: T = 293 K; $m_1 = 1000$ Da and m_2 = 58.44 Da; $\sigma_2 = 2 \times 10^{-4}$ m (Zheng et al., 2008); $n_1(0)$ is marked in Fig. 9; $\overline{u}$ is approximate to 0.5 m/s in the study area; ρ = 0.5 and $k = 1.38065 \times 10^{-23}$ J/K.

We use a four-point average method to calculate the mean turbidity from the MODIS reanalyzed data. The four points are four resolution cells surrounding a position at which the salinity data are taken. Comparison of the normalized mean turbidity data with the DOM distribution model is shown in Fig. 9. The correlation coefficient

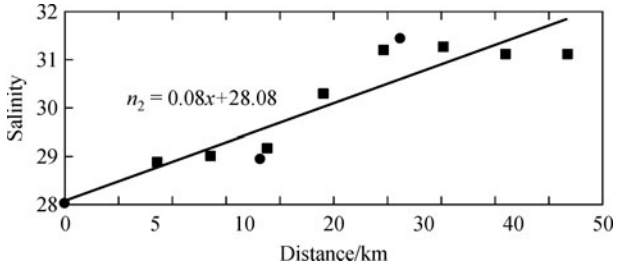

Fig. 8 Salinity data fitting. Circles represent salinity at the stations. Square represents salinity by interpolation.

between the normalized mean turbidity data and the model curve of 100 NTU reaches 0.96 (significant at the 95% level of confidence).

Based on the above results, we can conclude that the inelastic collision between the terrestrial DOM molecules and dissolved salt ions may cause the molecules to adhere to each other and form large size molecule groups; when the size grows large enough, the groups may sink toward the sea floor while changing their optic effect. The above process is a decisive dynamic mechanism causing the loss of the terrestrial DOM in coastal seawater. In other words, it is the salinity at a macro-scale which is a decisive factor that leads to the decrease of turbidity in coastal waters in our study area. Theoretically, terrestrial DOM from the Jiulongjiang River can reflect the path of the JRP. Therefore, we can use the seawater turbidity as another

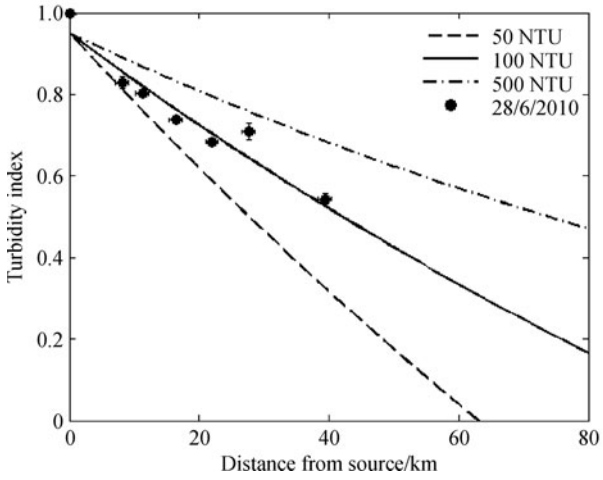

Fig. 9 Turbidity index distribution along the x-axis derived from the DOM distribution model (curves). The basic points and error bars are derived from the normalized MODIS turbidity by $n_1(0)$ on June 28, 2010. Three curves represent three cases of $n_1(0)$, including 50 NTU, 100 NTU and 500 NTU.

indicator for analysis of river plumes such as the JRP (Shi and Wang, 2009). Figure 7 clearly shows the status of the jets formed by the JRP on June 28, 2010. Meanwhile, the signal of coastal upwelling off Xiangzhi-Weitou characterizes a lower turbidity in Fig. 7 as compared to the turbidity of JRP.

5 Discussion

5.1 Plume indicators

From the above study, we see that the MODIS reanalyzed turbidity data provides a clear signal of the high-turbidity JRP. On the basis of the turbidity data from 2003 to 2011, we can obtain a turbidity distribution image (Fig. 10) which distinctly shows the presence of jets formed by the Xiamen JRP and JinWei JRP on June 28, 2010 (Fig. 7). This indicates that the jets developed by Xiamen JRP and JinWei JRP as those on June 28 are not fortuitous phenomena.

The natural indicator for freshwater plume in the coastal ocean is salinity, but salinity cannot be remotely sensed at useful spatial scales. Instead, turbidity can be another indicator used to track the behavior of river plumes in the coastal ocean. Comparing Fig. 2 with Fig. 7, one can see that the general spreading trends for the JRP are northeastward and southwestward, but there exists some difference between the in-situ salinity distribution and the turbidity distribution.

The elementary reasons follow. Firstly, the sources affecting the optical property of seawater are multiple nearshore, such as local resuspended sediment and the bank erosion. So, strictly speaking, the factors that determine the value of turbidity may be not just the Jiulongjiang River. Secondly, the transport of terrestrial DOM is complicated. Besides the inelastic collision between the DOM molecules and dissolved salt ions, photo-oxidation, mixing process, and bacterial degradation are also described as the mechanisms for the removal of terrestrial DOM (Wang et. al., 2004). So in the coastal area the river runoff is the most important factor that influences salinity, and as a tracer for river plume, salinity can display more detailed patterns in comparison with turbidity.

5.2 Four extension patterns for JRP

The ability to apply turbidity to map plumes allows

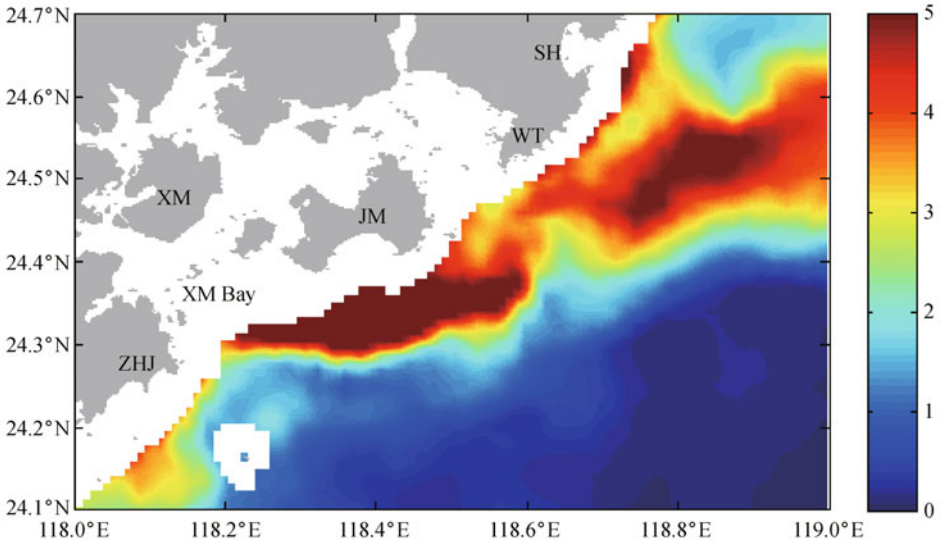

Fig. 10 MODIS reanalyzed turbidity distribution displaying the status of jets formed by the JRP as Fig. 7 on August 29, 2003. SH, WT, JM, XM, and ZHJ represent Shenhu, Weitou, Jinmen, Xiamen, and Zhenhaijiao, respectively.

analysis of spatial patterns of the Jiulongjiang River and helps to further description and understanding of the JRP. Due to the bio-optical, physical, and environmental complexities, it is not every day we can get the satellite-derived turbidity data on the study area, and not all of the distributions of turbidity can clearly display the signal of JRP.

In view of the turbidity distribution images on the days with distinct JRP signals from the year of 2003 to 2010, there are mainly four types of extending patterns for the JRP. First, going northward along the coastline (Figs. 11(a) and 12(a)) with the highest occurrence probability of 51%. Second, extending northeastward and southwestward at the same time (Figs. 11(b) and 12(b)), i.e., it is a bi-directional plume with the second largest occurrence probability of 20%. Third, just spreading out near the Xiamen Bay mouth (Figs. 11(c) and 12(c)) with 19% occurrence probability. The last but not the least , flowing northeastward offshore (Figs. 11(d) and 12(d)) with 10% occurrence probability. Figures 11 and 12 show the representative images and average images for the four patterns, respectively.

5.3 Theoretical approximation

In Section 3.2.1, we adopt the theory of a 2D jet (Kundu, 1990) as a physics model, which is used for interpretation of cruise observations. The 2D jet theory is derived based on the momentum balance between advection and lateral viscosity. In the coastal ocean, however, there is a possibility for strong coastal currents to destroy such momentum balance and modify the jet. In our case, from Figs. 2 and 5, one can see that in an area near the Xiamen Bay mouth, the diluted water plume patterns are indeed close to the theoretical 2D jet. Beyond this area, the plume axes have remarkable turning, indicating the forcing of coastal currents, but the plume structure still keeps a similarity to the 2D jet model. Thus, in our case, the 2D jet model is a rough approximation for interpretation of cruise observations.

Due to lack of current velocity data, we use the cruise-measured density field to inverse the x-component of velocity $u(y)$ using Eq. (10), $\rho_t = -\alpha u(y)$, where α is assumed to be a constant. Equation (10) is derived from the continuity equation in the form of

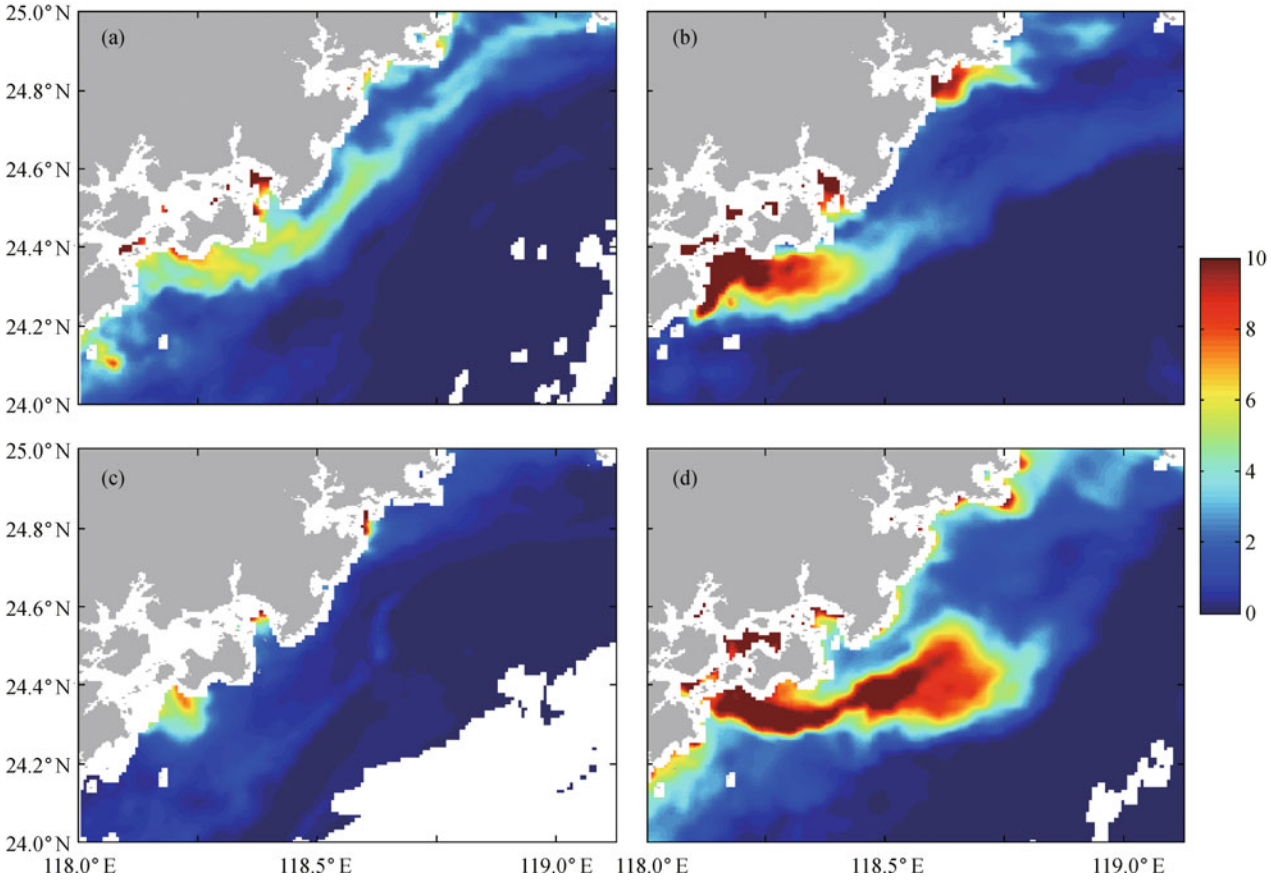

Fig. 11 Turbidity representative distributions for the four extension patterns of JRP. (a)–(d) are those on August 17 of 2010, July 26 of 2011, July 16 of 2005 and August 28 of 2003, respectively, with corresponding occurrence probabilities as follow: 51%, 20%, 19% and 10%.

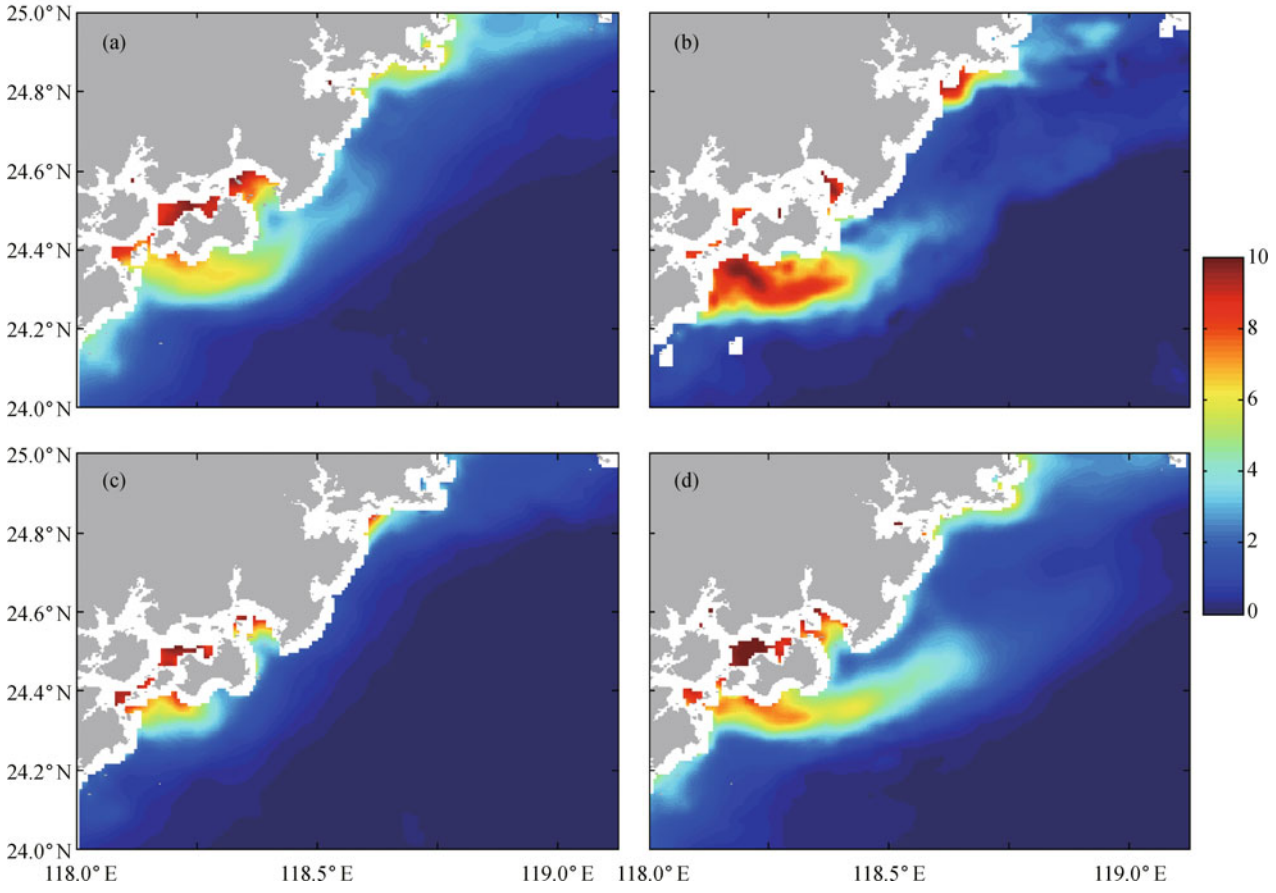

Fig. 12 Average distributions of turbidity for the four extension patterns of JRP. (a)–(d) are those going northward along the coastline, extending northeastward and southwestward at the same time, just spreading out near the Xiamen Bay mouth and flowing northeastward offshore, respectively.

$$\rho_t = -\frac{\partial \rho}{\partial x} u(y). \tag{13}$$

In general, ρ is a continuous function of x, assuming α ($=\partial\rho/\partial x$) to be a constant implies to take a linear approximation of $\rho(x)$.

6 Summary

We analyze the JRP based on the jet theory and the cruise observations carried out from June 28 to 30, 2010 in the west Taiwan Strait. The results indicate that in the 2 m layer, the JRP flows into the adjacent water through Xiamen Bay in the form of jets J0 and J1 in the southwestward and southeastward directions with angles of 151° and 90° to the direction of the coastline, respectively. Meanwhile, the JRP enters into the west Taiwan Strait through the channel between Jinmen and Weitou in the form of jet J2 whose axis directs northeastward with an angle of 9° to the direction of the coastline. Driven by the summer southwesterly monsoon, Dongshan low temperature and high salinity water runs northeastward into the survey area in the form of jet J3, with the jet axis at an angle of 9° to the direction of the coastline, whose intensity is the strongest as compared to other jets.

After entering into the west Taiwan Strait, the Xiamen JRP and JinWei JRP both take the shape of plume water with fronts. The maximum width of the JRP coverage is about 31.5 km, and the length is about 86.3 km in the 2 m layer. The isohalines are dense in the interaction zones of the jets and form salinity fronts with the salinity gradient up to 0.365/km.

In the 2 m layer, to some degree, the jets outside the Xiamen Bay are blocked by the strong jet J3, without flowing further offshore. The collision between J2 and J3 prevents the JinWei JRP from spreading southwestward or southeastward. The JinWei JRP, dragged by jet J3, extends northeastward. Vertically, jet J0 has an influence depth from 2 to 7 m, with a shorter axis length in its 7 m layer. It also shows that the JRP has an impact depth of less than 10 m.

Using the terrestrial DOM distribution model developed by Zheng et al. (2008), we analyzed the DOM degradation

in the study area. The correlation coefficient of the theoretical model to the MODIS turbidity data is 0.96 (significant at the 95% level of confidence). The results indicate that the inelastic collision between the terrestrial DOM molecules and dissolved salt ions in seawater is a decisive dynamic mechanism to cause the loss of terrestrial DOM in coastal regions. At the macro-scale, the salinity is a decisive factor for the diminishing of turbidity in the study area. Thus we can utilize the turbidity as an indicator to study the extension patterns of the JRP. For example, in the MODIS turbidity distribution image on June 28, 2010, one can clearly see the status of the jets formed by the JRP.

According to the MODIS reanalyzed turbidity data, there are mainly four spatial extending patterns for the JRP, which are listed from the highest occurrence probability to the lowest one. These include running northward along the coastline with the occurrence probability of 51%, a bi-directional plume with branches spreading northeastward and southwestward at the same time with the occurrence probability of 20%, just extending out near the Xiamen Bay mouth with 19% occurrence probability and flowing northeastward offshore with 13% occurrence probability.

Acknowledgements This work was jointly supported by the National Basic Research Program of China (No. 2009CB21208) and the National Natural Science Foundation of China (Grant Nos. 41276006, 41121091 and 40810069004). The authors would like to express their appreciation to the crew of R/V Yanping 2 and all of the cruise participants for help with the field work. We thank Ms. Yonghong Li for providing the MODIS satellite data, Mr. Zhenyu Sun and Ms. Jia Zhu for their insightful suggestions. Zheng also appreciates the financial support by a Key Program from the State Administration of Foreign Experts Affairs of China. We are grateful to two anonymous reviewers for their valuable suggestions and comments for improving the manuscript.

References

Chao S Y, Boicourt W C (1986). Onset of estuarine plumes. J Phys Oceanogr, 16(12): 2137–2149

Chen H, Hu J Y, Pan W R, Zeng G N, Chen Z Z, He Z G, Zhang C Y, Li H (2002). Underway measurement of sea surface temperature and salinity in the Taiwan Straits in August, 1999. Marine Science Bulletin, 4(1): 11–18

Chen J Q, Fu Z L, Li F X (1982). Study of upwelling in Minnan-Taiwan Bank. J Oceanogr Taiwan, 2(1): 5–13 (in Chinese)

Chen X H, Hu J Y, Pi Q L, Liu G P, Chen Z Z (2009). Densely underway measurement of surface temperature and salinity in Xiamen-Quanzhou near-shore area. Advances in Earth Science, 24(6): 629–635 (in Chinese)

Guo W D, Yang L Y, Hong H S, Stedmon C A, Wang F L, Xu J, Xie Y Y (2011). Assessing the dynamics of chromophoric dissolved organic matter in a subtropical estuary using parallel factor analysis. Mar Chem, 124(1–4): 125–133

Hickey B, Geier S, Kachel N, MacFadyen A (2005). A bi-directional river plume: the Columbia in summer. Cont Shelf Res, 25(14): 1631–1656

Hong H S, Zhang C Y, Shang S L, Huang B Q, Li Y H, Li X D, Zhang S M (2009a). Inter annual variability of summer coastal upwelling in the Taiwan Strait. Cont Shelf Res, 29(2): 479–484

Hong H S, Zheng Q A, Hu J Y, Chen Z Z, Li C Y, Jiang Y W, Wan Z W (2009b). Three-dimensional structure of a low salinity tongue in the southern Taiwan Strait observed in the summer of 2005. Acta Oceanol Sin, 28(4): 1–7

Huang Y C, LI Y, Shao H, Li Y H (2008). Seasonal variations of sea surface temperature, chlorophyll *a* and turbidity in Beibu Gulf, MODIS imagery study. Journal of Xiamen University (Natural Science), 47(6): 856–863

Kim H C, Yamaguchi H, Yoo S, Zhu J R, Okamura K, Kiyomoto Y, Tanaka K, Kim S W, Park T, Oh IS, Ishizaka J (2009). Distribution of Changjiang diluted water detected by satellite chlorophyll *a* and its interannual variation during 1998–2007. J Oceanogr, 65(1): 129–135

Kundu P K (1990). Fluid Mechanics. San Diego: Academic Press, 478–481

Libes S (2009). Introduction to Marine Biogeochemistry. San Diego: Academic Press, 208

Lie H J, Cho C H, Lee J H, Lee S (2003). Structure and eastward extension of the Changjiang River plume in the East China Sea. J Geophys Res, 108(C3 3077): 22, 1–14

Liu Y G, MacCready P, Hickey B M (2009a). Columbia River plume patterns in summer 2004 as revealed by a hindcast coastal ocean circulation model. Geophys Res Let, 36: L02601

Liu Y G, MacCready P, Hickey B M, Dever E P, Kosro P M, Banas N S (2009b). Evaluation of a coastal ocean circulation model for the Columbia River plume in 2004. J Geophys Res, 114(C2): C00B4

Liu Y G, Weisberg R H (2007). Ocean currents and sea surface heights estimated across the West Florida Shelf. J Phys Oceanogr, 37(6): 1697–1713

Luo Z B, Pan W R, Li L, Zhang G R (2011). Salinity fronts at Jiulongjiang Estuary. IEEE Remote Sensing, Environment and Transportation Engineering (RSETE), 3449–3454

Luo Z B, Pan W R, Li L, Zhang G R (2012). The study on three-dimensional numerical model and fronts of the Jiulong Estuary and the Xiamen Bay. Acta Oceanol Sin, 31(4): 55–64

MacCready P, Banas N S, Hickey B M, Dever E P, Liu Y G (2009). A model study of tide- and wind-induced mixing in the Columbia River Estuary and plume. Cont Shelf Res, 29(1): 278–291

Mao H L, Gan Z J, Lan S F (1963). A preliminary study of the Yangtze diluted water and its mixing processing. Oceanologia ET Limnologia Sinica, 5(3): 183–206 (in Chinese)

Ortner P B, Lee T N, Milne P J, Zika R G, Clarke M E, Podesta G P, Swart P K, Tester P A, Atkinson L P, Johnson W R (1995). Mississippi River flood water that reached the Gulf Stream. J Geophys Res, 100(C7): 13595–13601

Rong Z R, Li M (2012). Tidal effects on the bulge region of Changjiang River plume. Estuar Coast Shelf Sci, 97(20): 149–160

Schiller R V, Kourafalou V H, Hogan P, Walker N D (2011). The dynamics of the Mississippi River plume–impact of topography, wind and offshore forcing on the fate of plume waters. J Geophys Res, 116(C6): C06029

Shi W, Wang M H (2009). Satellite observations of flood-driven Mississippi River Plume in the spring of 2008. Geophys Res Lett, 36 (7): L07607

Wang X C, Chen R F, Gardner G B (2004). Sources and transport of

dissolved and particulate organic carbon in the Mississippi River estuary and adjacent coastal waters of the northern Gulf of Mexico. Mar Chem, 89(1–4): 241–256

Wu H, Zhu J R, Shen J, Wang H (2011). Tidal modulation on the Changjiang River plume in summer. J Geophys Res, 116(C8): C08017

Zhang C Y, Hong H S, Hu C M, Shang S L (2011). Evolution of a coastal upwelling event during summer 2004 in the southern Taiwan Strait. Acta Oceanol Sin, 30(1): 1–6

Zhang Y H, Wang W Q, Huang Z Q (1999). Salinity fronts and chemical behavior of nutrient in Jiulongjiang Estuary. Marine Environmental Science, 18(4): 1–7 (in Chinese)

Zheng Q A, Chen Q, Zhao H H, Shi J X, Cao Y, Wang D (2008). A statistic-thermodynamic model for the DOM degradation in the estuary. Geophys Res Lett, 35(6): L06604

Zheng Q A, Clemente-Colon P, Yan X H, Liu W T (2004). Satellite synthetic aperture radar detection of Delaware Bay plumes: Jet-like feature analysis. J Geophys Res, 109(C3): C03031

AUTHOR BIOGRAPHIES

Daifeng Wang is a Ph.D Candidate in the College of Ocean and Earth Sciences, Xiamen University, China. Her current research interests focus on river plume. E-mail: dfengw@xmu.edu.cn

Dr. Quan'an Zheng is a Senior Research Scientist of the Department of Atmospheric and Oceanic Science, University of Maryland, USA, and a Guest Chair Professor of Xiamen University, China. His research interests are ocean remote sensing (including physics, data interpretation, applications, and laboratory simulation), ocean surface processes (including wind friction, wave spectra, skin layer physics, and surfactant effects), upper ocean dynamics (including internal wave dynamics and ocean-atmospheric coupling), mesoscale ocean dynamics, and solitary waves in the atmosphere and ocean. E-mail: quanan@atmos.umd.edu. Website: http://www.atmos.umd.edu/~quanan/

Dr. Jianyu Hu obtained his Ph.D degree (2001) in physical oceanography from Tohoku University of Japan and Ph.D degree (2002) in environmental science from Xiamen University of China. He is now a professor in State Key Laboratory of Marine Environmental Science and Department of Physical Oceanography at Xiamen University, focusing on the study of regional environmental oceanography.